Design and Development of a Dexterous Tendon-Driven Robotic Hand

Hao Chen

haochen2880@gmail.com | (913) 215-4365

Companion force-analysis calculator: ActuationLab (actuationlab.dev)

Abstract

This report develops a preliminary architecture and sizing basis for a dexterous tendon-driven robotic hand. The system comprises 25 independently actuated degrees of freedom (DOF): 24 hand-and-wrist axes and one separate proximal forearm-rotation axis. Antagonistic tendons, predominantly forearm-mounted actuation, a detachable hand interface, and custom pancake outrunners are proposed to combine low distal inertia with controllable mechanical impedance. Quasi-static load models distinguish joint torque, tendon tension, spool torque, and motor-shaft torque, including explicit routing losses and transmission ratios. Example calculations, governing formulas, and step-by-step solution procedures are provided for sizing the finger and wrist actuators. Candidate motor geometries, windings, and thermal budgets are derived from these requirements; they are not validated actuator ratings. Prototype development and qualification address friction, tendon creep, calibration, backdrivability, thermal behavior, and task performance.

Contents

1 Design Scope and Requirements **1**
1.1 Motion Allocation and System Boundary . . . 1
1.2 Performance and Integration Requirements . . . 1

2 Mechanical Architecture and Transmission **2**
2.1 Antagonistic Tendons and Remote Actuation . . . 2
2.2 Detachable Hand Interface . . . 2
2.3 Finger Geometry and Structural Manufacturing . . . 3
2.4 Two-Axis Wrist and Proximal Forearm Rotation . . . 4
2.5 Tendon Routing, Guides, and Take-Up . . . 4
2.6 Wrist Timing-Belt Alternative . . . 5

3 Engineering Analysis and Calculations **6**
3.1 Notation, Assumptions, and Load Cases . . . 6
3.2 Joint Torque and Tendon Tension . . . 7
3.3 Transmission Losses and Reduction . . . 7
3.4 Finger Load Cases and Actuator Sizing . . . 7
3.5 Wrist Load Cases and Actuator Sizing . . . 8
3.6 Tendon Travel and Motor Speed . . . 10
3.7 Motor Geometry, Winding, and Thermal Sizing . . . 10
3.8 Consolidated Actuator Requirements . . . 12

4 Proposed Actuator and Control Design **12**
4.1 Pancake Outrunner Configuration . . . 12
4.2 Custom Windings and Speed Constant . . . 12
4.3 Rotor Bell and Magnetic Return Path . . . 13
4.4 Low-Ratio Reduction . . . 13
4.5 Per-Axis Field-Oriented Control and Electronics . . . 14
4.6 Direct Joint-Position Sensing and Tendon Calibration . . . 14

5 Tendon Materials and Transmission Qualification **15**
5.1 Candidate Materials and Selection Rationale . . . 15
5.2 Braid Geometry and Construction . . . 15
5.3 Creep, Constructional Settling, and Recovery . . . 16
5.4 Guide Friction and Wear . . . 16
5.5 Qualification Strategy . . . 17

6 Prototype Development and Verification **17**
6.1 Staged Prototype Development . . . 17
6.2 Standards and Benchmarking Basis . . . 17
6.3 Performance Test Matrix . . . 17
6.4 Calibration and Independent Verification . . . 18
6.5 Durability and Maintenance Qualification . . . 20
6.6 Task-Level Reporting . . . 20

References **21**

A Extended Calculations and Sensitivity **23**

B Calculated Sensitivity Plots **26**

C Supporting Tendon Evidence and Test Protocol **28**

D ActuationLab Calculator Reference **31**

1 Design Scope and Requirements

The project targets independently controlled grasping and assembly manipulation, including turning threaded components. The immediate development objective is to establish viable joint geometry, tendon routing, transmission losses, and calibration through PLA and servo-driven prototypes before committing to custom actuators and machined structures. This report presents a preliminary design and analytical load cases; measured prototype performance is not yet reported.

1.1 Motion Allocation and System Boundary

The baseline has 24 hand-and-wrist axes and one proximal forearm-rotation axis, with one motor and dedicated motor-control PCB per axis. The 22 finger, thumb, and palm axes use antagonistic tendon pairs. Tendon-driven wrists raise that total to 24 pairs; a synchronous belt may replace either wrist pair. The proximal rotation transmission is sized independently.

Table 1: Proposed active degrees of freedom.

Region	**Active motions**	**DOF**
Each non-thumb finger	DIP flexion–extension; PIP flexion–extension; MCP flexion–extension and abduction–adduction	4 per finger
Thumb	Four independently controlled motions, with an additional rotational motion contributing to opposition; anatomical allocation to be finalized	5
Little-finger side of the palm	Fifth carpometacarpal (CMC) flexion contributing to palm cupping	1
Wrist	Flexion–extension and radial–ulnar deviation (abduction–adduction)	2
Proximal forearm, near elbow	Axial forearm rotation corresponding to pronation–supination	1
Total	**Hand and wrist: 24; proximal forearm rotation: 1**	**25**

The thumb allocation is fixed at five active axes for system sizing; its detailed joint geometry will be established in the kinematic model. The two wrist axes and proximal forearm rotation are distinct mechanisms, as described in Section 2.4.

1.2 Performance and Integration Requirements

- Independent active control of every allocated axis, including bidirectional torque and verified tendon engagement over the operating range.
- Low distal mass through predominantly forearm-mounted motors; a detachable hand interface compatible with successive actuator assemblies.
- Low breakaway torque and transmission hysteresis, with backdrivability assessed at the joint and fingertip rather than inferred from motor or gearbox type.
- Adjustable tendon take-up, accessible wear components, and repeatable recalibration after hand

or actuator replacement.

- Force, speed, accuracy, temperature, and maintenance limits tied to specified tasks and duty cycles. The human-reference cases in Section 3 are sizing inputs, not demonstrated dexterity or continuous-duty ratings.

2 Mechanical Architecture and Transmission

The proposed mechanism combines antagonistic tendon actuation, CNC-machined aluminum finger structures, a two-axis wrist, and a separate proximal forearm-rotation stage. The architecture is selected for independent manipulation with low finger inertia; the following subsections retain the engineering rationale and the principal tradeoffs.

2.1 Antagonistic Tendons and Remote Actuation

Each spool retracts one tendon while paying out its antagonist. Routing must preserve useful moment arms, adequate payout, and engagement while limiting cross-axis coupling. Hand and wrist motors are principally mounted on the rotating forearm structure; small palm-mounted actuators remain possible where thumb or palm routing becomes impractical.

2.1.1 Rationale for Antagonistic Tendon Pairs

One motor per pair provides active motion in both directions without a separate return actuator. The objective is for external joint motion to reach the actuator through a low-loss transmission, making motor and drive behavior the principal determinants of backdrivability. Tendon friction, compliance, and hysteresis constrain this objective. Pair pretension is established mechanically; a single motor does not independently control both branch tensions.

2.1.2 Rationale for Forearm-Mounted Actuation

Remote motors reduce finger inertia and permit larger actuators, improved heat removal, and service access. These benefits justify the additional routing and calibration burden. Joint-mounted motors were rejected as the default because their mass and packaging requirements would be carried by the moving digits.

2.2 Detachable Hand Interface

The hand will connect to the forearm through repeatable mechanical alignment, positive retention, and identified tendon and electrical connections. Disconnection requires controlled release of tension; reconnection must restore tendon pairing, pretension, encoder references, and travel limits. Interface geometry must accommodate the two-axis wrist without requiring complete tendon rethreading.

2.2.1 Rationale for Modular Prototyping

Separating the hand from its actuator assembly allows finger geometry and actuation hardware to evolve independently. Forearm-mounted servos support rapid early iteration; custom brushless motors can replace them while retaining the verified hand interface. The same arrangement supports replacement of damaged hand modules, subject to calibration checks after every exchange.

2.3 Finger Geometry and Structural Manufacturing

The baseline provides four independent axes per non-thumb finger. The proposed flexion joints would pass through the straight configuration and bend toward either side of the hand. An initial design target is approximately 45° of backward travel beyond straight at each finger flexion joint, with the mechanical extension stop placed at the end of that travel. With straight defined as 0° and forward flexion positive, the proposed extension reference is approximately −45°. This changes joint range rather than DOF count. The usable range must be established for each axis from clearance, tendon engagement and leverage, available payout, sensor accommodation, and structural testing.

2.3.1 Rationale for Bidirectional Finger Motion

Dorsal-side grasping could reduce wrist reorientation and increase approach options. Its value depends on thumb opposition, contact geometry, and retained tendon leverage in reverse bending. PLA prototypes will compare palm-side and dorsal-side grasp tasks before the geometry is committed to machined parts.

Additional backward travel is also intended to give a finger room to yield under an external impact before reaching its mechanical stop. Overtravel alone does not establish backdrivability: tendon and guide friction, gearing, reflected motor inertia, and the controller's commanded impedance determine resistance to externally imposed motion. Normal commanded motion will retain clearance from the mechanical travel limits. A compliant bumper may cushion contact at the ultimate stop. Homing will use a repeatable mechanical seating condition, with any bumper compression and transmission deflection included in the reference-repeatability check. The proposed 45° allowance is a development target rather than a demonstrated impact-protection rating. Controlled impact and forced-overtravel tests shall quantify peak loads, usable travel, damage, and calibration change, including powered and unpowered actuator behavior.

2.3.2 Rationale for Rigid Palm Supports

The palm shall use rigid metacarpal support structures at the MCP joint mounting interfaces, without intentional passive flexure. This is intended to maintain stable knuckle-axis locations and orientations and improve fingertip positioning repeatability. Bending of these supports under changing joint configurations and loads can alter the finger-base geometry and produce unintended fingertip deviations. Structural stiffness and mounting integrity shall therefore be evaluated against the fingertip positioning-error budget. The proposed little-finger-side palm-cupping motion remains a discrete, actively controlled joint between rigid structures, rather than distributed flexing of the palm supports.

2.3.3 Rationale for Structural Materials

PLA supports rapid geometry and routing changes. CNC-machined aluminum is the preferred final finger material because accurately located bearings and guides can be combined with load-directed material removal. Alloy, wall thickness, and fatigue performance require structural validation. SLS remains an option for components whose geometry or function favors it; manufacturing method is selected per component.

2.4 Two-Axis Wrist and Proximal Forearm Rotation

Two approximately orthogonal bearing-supported wrist axes provide flexion–extension and radial–ulnar deviation. Each has one motor and either an antagonistic tendon pair or a reversible synchronous-belt stage. A separate axial rotation joint near the elbow functionally provides pronation–supination. Finger and wrist actuator mounts rotate with the forearm to avoid twisting the tendon bundle relative to the hand. Travel limits and cable accommodation are required at the proximal rotary interface; continuous rotation is not assumed.

2.4.1 Rationale for Separating Forearm Rotation

Moving axial rotation proximally simplifies the wrist while retaining three orientation axes across the complete assembly. The tradeoff is the inertia of the forearm structure and its mounted actuators, which must be included in the proximal drive calculation. The wrist calculations do not size that drive.

2.5 Tendon Routing, Guides, and Take-Up

The proposed finger tendons use Sufix 832 braided line, as discussed in Section 5, and will be routed within polytetrafluoroethylene (PTFE) tubing along the transmission paths. Tendons and tubing will be integrated predominantly inside the hand structure, using internal channels and protective covers to minimize exposed spans that could be snagged or cut during manipulation. Tendon paths shall run through the central interior of each non-thumb finger, with eight tendons emerging at the metacarpophalangeal (MCP) knuckle interface: four antagonistic pairs, comprising two tendons per motor for the four independently controlled axes. Each tendon shall occupy an individual, identifiable routing channel. Channel identifiers shall map each tendon to its motor, controlled joint axis, and actuation direction, supporting correct assembly, tensioning, and replacement. Central internal routing shall retain the required tendon offsets at the driven joints to generate torque. Joint transitions and service openings will preserve the required motion range and access for tendon replacement.

Tendon allocation. The four non-thumb fingers require 32 tendons (8×4), the five-axis thumb requires 10 tendons, and little-finger-side palm cupping requires two tendons, giving 44 tendons within the hand. Each of the two wrist axes would add an antagonistic pair, giving four additional tendons and a total of 48 for a fully tendon-driven hand and wrist. A timing-belt transmission may replace the tendon pair on either wrist axis; belt spans are not counted as additional tendons. The separate proximal forearm-rotation stage is excluded from this count.

Tubing friction, bend radius, and wear will be evaluated for the complete routed assembly; the fixed-guide calculations alone do not quantify these additional losses.

Early prototypes route tendons over stainless-steel dowels at the finger joints. Effective tendon moment arm is determined by the tendon line of action, not the dowel-center offset alone. Ball-bearing-supported pulleys or guides are proposed for the final route.

Joint-decoupling verification. Prototype testing shall verify that moving one joint does not change the tendon path lengths associated with other independently controlled joints. Each joint shall be swept through its intended range in both directions while the remaining joints are held fixed and actuator compensation is disabled. Required tendon payout for the inactive axes shall be measured under controlled pretension, including representative wrist configurations. The target is no measurable cross-axis path-length change within the stated measurement resolution. Any detected coupling shall be quantified and addressed through routing revisions and retesting.

2.5.1 Actuator-Mounted Ratcheting Take-Up

A ratcheting tendon take-up mechanism is proposed on top of the actuator, at its output interface, for use with both prototype servos and the later brushless actuator assemblies. The tendon would make two complete wraps around the take-up horn or spool. When assembly settling or creep introduces slack, the user would engage the horn with a key and turn it to incrementally take up excess tendon length and restore pretension. The ratchet would retain the adjusted position after the key is removed, providing manually initiated tension adjustment without rethreading the tendon.

The take-up adjustment must act relative to the actuator output so that it changes the tendon-length setting rather than simply moving the joint. During normal operation, the actuator must remain able to pull one branch and release the opposing branch. Retensioning will balance the antagonistic pair at a defined joint reference while avoiding unnecessary tendon and bearing loads. Prototype testing will establish adjustment resolution, resistance to slip or unintended ratchet release, retention under reversing loads, and any change in joint zero after adjustment.

2.5.2 Rationale for Rolling Guides and Adjustable Tensioning

Rolling guides are intended to reduce sliding friction and wear while maintaining defined routing. Bearing drag, seal resistance, tendon bending, and packaging still contribute losses. Mechanical take-up restores engagement after settling or creep but cannot eliminate load-dependent compliance. Selection therefore depends on route-level friction, wear, and drift tests rather than guide type alone.

2.6 Wrist Timing-Belt Alternative

A local closed synchronous belt can replace a wrist tendon pair, with its two spans providing reversible torque transmission. The two-axis support frames must preserve pulley alignment as the other wrist axis moves. The initial 20/60-tooth, 3 mm-pitch layout is evaluated in Section 3.5; belt width and installation tension require manufacturer load-rating checks.

2.6.1 Rationale for the Belt Candidate

Positive tooth engagement and a catalog-rated tensile system may suit the wrist's higher loads. The tradeoffs are pulley volume, installation tension, bearing load, reversal compliance, and axis-

alignment constraints. Higher force alone does not establish superiority over a properly sized tendon. Adjustable tensioning locked after setup is preferred for initial reversing-drive trials [22]; tooth clearance, cord stretch, and tooth deformation remain positioning-error sources [23].

3 Engineering Analysis and Calculations

ActuationLab (actuationlab.dev) is the companion interactive calculator for the force and preliminary motor-sizing analyses in this paper. Its force workspace accepts finger geometry and posture, external loads, tendon and spool radii, pretension, routing losses, reduction, and design factors. It calculates joint moments, branch tensions where resolved by the loss model, spool and motor-shaft torque requirements, travel, and average speed. Inverse load capacity, sensitivity plots, and optional measured-material checks support comparison of candidate transmissions.

The motor-design workspace carries a selected axis's shaft requirement into comparisons of speed constant, current, copper heating, stator diameter and stack length, winding construction, and reflected rotor inertia. Geometry results state the electromagnetic loading required; they do not predict a motor's demonstrated torque capability. The derivations, assumptions, and worked examples that follow provide the underlying mathematics and steps needed to reproduce the website's results. Appendix D defines every input and output, the available workflows, and the interpretation limits. The website remains a compact calculation interface; the detailed reference is retained in this paper.

3.1 Notation, Assumptions, and Load Cases

The initial sizing model is quasi-static and uses equal opposing tendon moment arms and spool radii, with both branches engaged. All reported required motor torques include a design factor $SF = 1.5$ unless identified as nominal. Acceleration, gravity, contact location, and combined-axis loading must be evaluated for the actual task; peak biological strength is not a continuous thermal requirement.

Table 2: Notation and baseline transmission assumptions. Dimensions refer to effective tendon or pulley pitch radii.

Quantity	**Finger example**	**Wrist tendon example**
Joint tendon moment arm r (mm)	8	30
Gearbox-output spool radius r_s (mm)	5	10
Gearbox speed reduction $G = \omega_m/\omega_s$	5	6
Forward gearbox efficiency η_g	0.85	0.85
Routing loss model	Capstan, $\mu_s = 0.071$, $\Theta = \pi$	Aggregate $\eta_t = 0.90$
Joint-side return tension T_p (N)	10	25
Design factor SF	1.5	1.5

External fingertip force is $\boldsymbol{F}$, joint coordinates are $\boldsymbol{q}$, joint moment is τ_i, and d_i is the effective external moment arm for the specified loading direction. Subscripts m, s, and j denote motor, spool, and joint. Angles in analytical expressions are radians. The finger proxy represents incipient sliding over fixed steel guides; the wrist efficiency represents proposed rolling routing. They are alternative loss models, not factors to multiply together.

3.2 Joint Torque and Tendon Tension

For a pure fingertip force, the signed moment about axis $\hat{\boldsymbol{e}}_i$ is

$$\tau_i = \hat{\boldsymbol{e}}_i \cdot \left[(\boldsymbol{p}_{\text{tip}} - \boldsymbol{p}_i) \times \boldsymbol{F}\right], \qquad \boldsymbol{\tau} = J(\boldsymbol{q})^T \boldsymbol{F}. \tag{1}$$

The planar magnitude reduces to $|\tau_i| = Fd_i$. For equal opposing tendon moment arms,

$$\tau_i = r_i(T_{+,j} - T_{-,j}), \qquad \Delta T_j = \frac{\tau_i}{r_i}, \qquad T_{\text{pull},j} = T_p + \frac{|\tau_i|}{r_i}. \tag{2}$$

Pretension and routing determine maximum individual tension; differential tension alone is insufficient for tendon or termination selection. A constant T_p is an assumed maintained return tension, not a prediction of the tensioner or compliant assembly. Variable moment arms and cross-joint routing require the corresponding tendon Jacobian.

3.3 Transmission Losses and Reduction

For fixed guides, let $a = \sum_j \mu_{s,j}\Theta_j$. At incipient sliding the capstan limit is $T_{\text{high}}/T_{\text{low}} = e^a$. With equal exponents on both branches and positive joint load,

$$T_{\text{pull},s} = e^a(T_p + \tau_i/r_i), \qquad T_{\text{return},s} = e^{-a}T_p, \tag{3}$$

$$\tau_{s,i} = r_{s,i}\left[e^a(T_p + \tau_i/r_i) - e^{-a}T_p\right], \qquad \tau_{m,\text{req},i} = \frac{SF\,\tau_{s,i}}{G\eta_g}. \tag{4}$$

The static proxy $\mu_s = 0.071$ comes from Dyneema-fibre/stainless-steel measurements [7]; it has not been measured for Sufix 832. Below the slip limit the tension ratio can be smaller; steady sliding requires measured kinetic friction. Reversal and unequal routes require separate branch treatment. Tendon bending losses are not resolved by this idealization.

For rolling routing represented by an aggregate forward efficiency η_t,

$$N_{m:j} = G\frac{r_i}{r_{s,i}}, \qquad \tau_{s,\text{req}} = \frac{SF\,\tau_i r_s}{r_i \eta_t}, \qquad \tau_{m,\text{req}} = \frac{SF\,\tau_i}{N_{m:j}\eta_g\eta_t}. \tag{5}$$

Motor-to-joint reduction includes both gearbox and pulley geometry. Forward efficiency does not establish reverse-drive resistance. Ideal reflected motor inertia is $N_{m:j}^2 J_m$, with additional gear, pulley, and structural inertia to be included.

3.4 Finger Load Cases and Actuator Sizing

Shinohara et al. reported index-finger maximum voluntary distal-phalanx flexion force of 32.4 ± 7.3 N across their age and gender groups [6]. The rounded 30 N reference and 15/60 N comparison cases below are task-specific load scenarios, not population percentiles or sustained-force ratings. The representative MCP flexion case uses $d = 80$ mm and the finger parameters in Table 2.

At 30 N, $\tau_j = 30(0.080) = 2.40$ N m and $\Delta T_j = 300$ N. With $T_p = 10$ N and $e^a = 1.2499$, spool-side tensions are approximately 387.5 and 8.0 N. Their difference produces 1.897 N m nominal spool torque; applying SF gives 2.846 N m at the gearbox output and 0.670 N m at the motor shaft. Tendon strength allowances are assessed separately from nominal tensions in the table.

Table 3: Illustrative force sizing with stationary stainless-steel dowels. All geometry and transmission values are assumptions.

Quantity	**Below**	**Reference**	**Above**
Fingertip force F_{tip} (N)	15	30	60
Joint torque τ_i (N m)	1.20	2.40	4.80
Joint tension difference ΔT_i (N)	150	300	600
Joint-side pulling tension (N)	160	310	610
Spool-side pulling tension (N)	200.0	387.5	762.4
Spool torque $\tau_{s,i}$, before SF (N m)	0.960	1.897	3.772
Required spool torque, with SF (N m)	1.440	2.846	5.658
Required motor torque, with SF (N m)	0.339	0.670	1.331

3.4.1 Joint-Specific Flexion and Lateral Loading

For a straight finger under a transverse fingertip load, DIP, PIP, and MCP leverage includes the distal segment, the distal two segments, and the full finger, respectively. The example moment arms are 25, 50, and 80 mm; they are not measured anatomical dimensions. Transmission parameters remain fixed to isolate the effect of external leverage.

Table 4: Illustrative separate finger-axis load cases at 30 N fingertip force. Moment arms are assumed; the lateral force is not a human-strength benchmark.

Joint axis	d_i **(mm)**	**Joint torque (N m)**	**Motor torque (N m)**
DIP flexion	25	0.750	0.215
PIP flexion	50	1.500	0.422
MCP flexion	80	2.400	0.670
MCP abduction–adduction	80	2.400	0.670

The MCP abduction–adduction row is a separate 30 N lateral load case, using the same 80 mm external and 8 mm tendon moment arms. It therefore yields the same calculated motor torque as flexion. The flexion study does not establish human lateral strength, and the two force components are not simultaneous parts of a single 30 N load. Actual axis sizing uses Equation (1) over the operating workspace. Smaller distal motors are plausible under comparable transmissions, but routing losses, acceleration, and thermal duty can change the ordering.

3.5 Wrist Load Cases and Actuator Sizing

Delp et al. measured wrist isometric strength across wrist angles in ten healthy adult males, with body and forearm constrained, shoulder abducted 90°, and elbow flexed 90° [21]. Table 5 uses half, equal, and twice the reported cohort mean peak moments. These are engineering comparison cases, not a universal population average, continuous rating, or simultaneous two-axis capacity.

The tendon candidate uses $r_w = 30$ mm, $r_s = 10$ mm, $G = 6$, and assumed $\eta_t = 0.90$. Total motor-to-wrist reduction is 18:1. For reference flexion,

$$\tau_{s,\text{req}} = \frac{1.5(12.2)(10/30)}{0.90} = 6.778 \text{ N m}, \qquad \tau_{m,\text{req}} = \frac{6.778}{6(0.85)} = 1.329 \text{ N m}. \tag{6}$$

Table 5: Wrist-joint torque targets based on a selected human cohort. Values are N m before transmission sizing and safety allowance.

Motion direction	**Below** (0.5×)	**Reference** (1×)	**Above** (2×)
Flexion	6.10	12.20	24.40
Extension	3.55	7.10	14.20
Radial deviation / abduction	5.50	11.00	22.00
Ulnar deviation / adduction	4.75	9.50	19.00

Table 6: Calculated wrist motor-shaft torque before reduction, including the stated losses and safety factor. Values are N m.

Motion direction	**Below**	**Reference**	**Above**
Flexion	0.664	1.329	2.658
Extension	0.387	0.773	1.547
Radial deviation / abduction	0.599	1.198	2.397
Ulnar deviation / adduction	0.517	1.035	2.070

Flexion governs the flexion–extension actuator; radial deviation governs the lateral actuator for these cases. Changing the gearbox to 4:1 or 8:1 gives 1.993 or 0.997 N m for reference flexion, with total reductions of 12:1 or 24:1. The proposed 6:1 gearbox is a compromise; its 18:1 total ratio reflects motor inertia by a factor of 324.

At reference flexion, joint-side tension difference is 406.7 N and the nominal pulling tension is 431.7 N with a 25 N return. Applying the 1.5 factor to the external torque raises the joint-side pulling value to 635 N; the doubled-reference case gives 1245 N. Absolute tensions elsewhere require a branch-level routing model: aggregate efficiency determines an equivalent tension difference, not each branch tension. Finger-line size cannot be assumed adequate for these wrist loads.

3.5.1 Timing-Belt Calculation

For the 20/60-tooth, 3 mm-pitch candidate, pitch radii $Zp/(2\pi)$ are 9.55 and 28.65 mm. With the 6:1 gearbox the total ratio remains 18:1. Substituting an assumed belt efficiency $\eta_b = 0.95$ for η_t gives

$$\tau_{m,\text{belt}} = \frac{1.5\tau_w}{18(0.85)(0.95)} = 1.259 \text{ N m} \quad (\tau_w = 12.2 \text{ N m}). \tag{7}$$

The doubled-reference value is 2.518 N m. Nominal span-tension difference at the large pulley is 426 N at reference and 852 N at twice reference, before the design factor and local losses. The apparent improvement depends on assumed efficiency. Pitch, width, engaged teeth, tensile-cord capacity, tooth ratcheting, installation tension, and bearing reaction must pass the manufacturer's sizing procedure [22].

3.6 Tendon Travel and Motor Speed

For constant moment arms and equal opposing spool radii,

$$\Delta L_i = r_i|\Delta\theta_i|, \qquad \Delta\phi_s = \frac{\Delta L_i}{r_{s,i}}, \qquad \overline{n}_m = \frac{60G\Delta\phi_s}{2\pi t}. \tag{8}$$

For tendons spanning multiple joints, $\Delta \boldsymbol{L} \approx J_t(\boldsymbol{q})\Delta\boldsymbol{q}$ locally; the full path must be integrated for finite motions. The examples below specify average speeds, not trajectory peaks or sourced human-speed benchmarks.

Table 7: Illustrative travel and speed requirements for 0.5 s moves.

Axis example	**Joint travel**	**Tendon (mm)**	**Spool travel**	**Motor RPM**
Finger	90°	12.57	144°	240
Wrist flexion–extension	60°	31.42	180°	360
Wrist radial–ulnar	30°	15.71	90°	180

3.7 Motor Geometry, Winding, and Thermal Sizing

Using the torque-control convention documented by ODrive [1],

$$K_t \approx \frac{8.27}{K_V}, \qquad \tau_m \approx K_t I_q, \qquad P_{\mathrm{Cu}} = \frac{3}{2}R_\phi I_q^2. \tag{9}$$

Here K_V is in RPM/V, K_t in N m/A, and I_q is peak-amplitude q-axis current with $I_d = 0$; phase RMS current is $I_q/\sqrt{2}$. Star line-to-line resistance is $2R_\phi$. Manufacturer constants using other current or commutation definitions must be converted before comparison [18]. Resistance and current limits are evaluated at operating temperature [19].

For an ideal rewind at fixed magnetic geometry, connection, mean turn length, and copper fill, increasing series turns by α approximately gives $K_t \propto \alpha$, $K_V \propto 1/\alpha$, conductor area $A_w \propto 1/\alpha$, and $R_\phi \propto \alpha^2$. At equal torque, $I_q \propto 1/\alpha$, so ideal copper loss is unchanged [17]. Real fill and end-turn penalties can change this result. The extended winding example is retained in Appendix A.

For radial-flux geometry, average air-gap shear stress σ_t gives

$$\tau_m \approx \frac{\pi}{2}\sigma_t D_g^2 L_s, \qquad R_{\phi,\max} = \frac{P_{\mathrm{Cu,allow}}}{1.5I_q^2}, \qquad K_{m,\min} = \frac{\tau_m}{\sqrt{P_{\mathrm{Cu,allow}}}}. \tag{10}$$

The geometry relation is a required-loading screen, not a torque prediction. At $D_g \approx D_s$, the proposed 60-by-15 mm finger stator needs 7.90 kPa for 0.670 N m; the 80-by-20 mm wrist stator needs 6.61 kPa for 1.329 N m. Detailed diameter/stack sweeps are in Appendix A.

The wrist's doubled-reference load requires 19.28 A I_q at 60 K_V and produces 100 W copper loss if hot resistance equals the stated limit. It is an overload development target until duty-specific thermal testing establishes an allowable duration or continuous capability. Budgets exclude iron, bearing, cable, gearbox, and PCB losses. Voltage margin requires measured back EMF, resistance, inductance, and inverter modulation at the required speed. A stationary hold can be thermally limiting despite zero mechanical output power.

Table 8: Electrical and thermal screening at the governing reference motor loads. All budgets and winding constants are candidate assumptions.

Quantity	**MCP candidate**	**Wrist candidate**
Motor-shaft torque (N m)	0.670	1.329
Candidate K_V (RPM/V)	80	60
Estimated K_t (N m/A)	0.1034	0.1378
Required I_q (A)	6.48	9.64
Phase RMS current (A)	4.58	6.82
Assumed copper-loss budget (W)	15	25
Maximum hot phase resistance (Ω)	0.238	0.179
Maximum hot star line-to-line resistance (Ω)	0.476	0.359
Minimum K_m (N m/$\sqrt{\text{W}}$)	0.173	0.266

Table 9: Calculated motor-shaft torque by actuator family. All entries include the stated loss model and $SF = 1.5$; they are not validated continuous ratings.

Axis	**Reference (N m)**	**Upper case (N m)**	**Total ratio**
DIP flexion	0.215	0.422	8:1
PIP flexion	0.422	0.835	8:1
MCP flexion	0.670	1.331	8:1
MCP abduction–adduction	0.670	1.331	8:1
Wrist flexion–extension	1.329	2.658	18:1
Wrist radial–ulnar	1.198	2.397	18:1

3.8 Consolidated Actuator Requirements

Finger upper cases use 60 N with the same moment arms and route; the lateral force remains an assumed design load. Wrist upper cases double the selected cohort means. Each assembled axis requires independent torque–speed and thermal verification. Thumb, palm, and proximal forearm motors retain symbolic load requirements until their geometry and task loads are defined; applying the MCP or wrist ratings to them would not constitute sizing.

4 Proposed Actuator and Control Design

4.1 Pancake Outrunner Configuration

The proposed custom actuator combines a short axial-length brushless outrunner, an application-specific winding, a low-ratio reducer, and a dual-direction tendon spool. Table 10 defines initial electromagnetic design points for the most demanding finger flexion axis and the wrist. These dimensions are inputs to electromagnetic, thermal, and packaging studies; they are not validated motor ratings. Smaller DIP and PIP variants should follow the axis-specific requirements in Section 3.4.1.

4.1.1 Rationale for the Outrunner Geometry

A larger air-gap radius increases the torque arm and the available electromagnetic surface area. The shear-stress model in Equation (10) makes the resulting diameter dependence explicit. A pancake arrangement also offers a short axial package around which a reducer may be integrated. These benefits must be balanced against rotor inertia, radial packaging, bearing support, cooling, and magnet retention. Increasing diameter alone does not establish a continuous torque capability.

Table 10: Initial custom motor design points. Stator dimensions are outer diameter and active stack length.

Parameter	MCP finger actuator	Wrist actuator
Stator diameter × active length	60 × 15 mm	80 × 20 mm
Speed constant K_V	80 rpm/V	60 rpm/V
Nominal bus voltage	24 V	24 V
Candidate slots / poles	12 / 14	24 / 28
Gear reduction G	5:1	6:1
Total motor-to-joint ratio N	8:1	18:1
Reference motor torque	0.670 N m	1.329 N m
Illustrative copper-loss budget	15 W	25 W

4.2 Custom Windings and Speed Constant

Winding turns, conductor cross-section, parallel strands, slot fill, and connection will be selected together to meet torque, speed, voltage, and thermal constraints. The proposed K_V values increase torque per ampere relative to a higher-K_V winding of the same convention, while retaining speed

margin for the illustrative motions in Section 3. Exact turns and wire sizes require the slot geometry, magnetic design, available end-turn space, and measured hot resistance.

4.2.1 Rationale for Application-Specific Windings

The objective is to match the available current and voltage to the required operating envelope. Lower K_V commonly requires more turns and a smaller conductor cross-section within a fixed slot, increasing resistance. It does not inherently reduce efficiency: under ideal constant-fill rewinding, the reduction in required current offsets the resistance increase at equal torque. Departures from equal fill, longer end turns, temperature rise, and iron losses determine the actual result [16, 17]. The calculation and counterexample are retained in Appendix A.

4.3 Rotor Bell and Magnetic Return Path

A ferromagnetic back-iron ring behind the magnets is proposed to complete the flux return path. Ordinary printed polymer and machined aluminum do not substitute magnetically for suitable steel. CNC machining is preferred for concentricity, magnet seats, bearing alignment, and air-gap control; the magnetic benefit comes from material properties and geometry, not the machining process itself. An aluminum hub or a suitably qualified printed carrier could support a separate steel ring.

4.3.1 Rationale for a Separate Back-Iron Specification

Insufficient thickness can cause saturation, while excessive thickness adds inertia without proportional torque benefit. Electromagnetic analysis must determine the steel grade and ring thickness and assess harmonic losses [20]. Mechanical qualification must address temperature, balance, centrifugal loading, and magnet retention. A solid machined ring is a candidate construction, not an efficiency guarantee.

4.4 Low-Ratio Reduction

A conventional gear reduction is the baseline packaging option; a planetary arrangement remains an alternative if its torque density or support geometry justifies the additional parts and mass. The reduction should be no larger than required by motor torque, thermal limits, and operating speed. The initial 5:1 and 6:1 values are calculation assumptions rather than final selections.

4.4.1 Rationale for Limited Reduction

Lower reduction limits reflected motor inertia and generally reduces the number of frictional interfaces affecting backdrivability. The complete ratio includes the spool-to-joint geometry, so gearbox ratio alone is insufficient. Efficiency under forward drive does not establish reverse-drive resistance. Selection will therefore use measured breakaway torque, hysteresis, backlash, stiffness, mass, and fatigue performance; a heavier planetary reducer is unnecessary if a simpler gear train meets the measured duty requirements.

4.5 Per-Axis Field-Oriented Control and Electronics

Each motor will have a custom control PCB implementing field-oriented control (FOC), rotor-position feedback, phase-current measurement, and temperature monitoring. The board design must account for current-sensor range and bandwidth, switching losses, bus decoupling, electromagnetic compatibility, regenerative energy, and protection limits. A provisional wrist power stage capable of approximately 30 A peak phase current provides design headroom above the 19.3 A illustrative upper-target demand, but allowable duration must follow device, winding, and thermal qualification.

4.5.1 Rationale for Independent Current Control

Independent torque-producing current regulation permits axis-specific force limits, compliant behavior, and consistent characterization across different windings. Current-based load estimates depend on calibrated torque constants and a model of gearing and transmission losses. They cannot distinguish external load from all friction, inertia, cogging, and tendon effects without additional information. Joint sensing and independent load measurements are therefore required to validate the estimate and detect transmission drift.

4.6 Direct Joint-Position Sensing and Tendon Calibration

Miniature, non-contact absolute magnetic angle sensing is proposed at each independently controlled finger axis. A small permanent magnet would rotate with one joint member, while a sensor on the adjacent member measures their relative angle. The four non-thumb fingers require 16 measured joint coordinates; the five thumb coordinates require sensing appropriate to their final mechanical allocation. Both MCP flexion–extension and abduction–adduction must be observable: a single flexion measurement cannot establish the two-axis configuration. Joint angles combined with the calibrated kinematic model provide an estimate of fingertip pose.

4.6.1 Rationale for Direct Output Feedback

Tendon stretch, creep, friction, and lost motion can make joint position differ from the position inferred from motor rotation. Measuring the joint directly allows this discrepancy to be observed and corrected within the available actuator and tension limits. Non-contact sensing avoids a sliding electrical contact at the joint. Joint feedback complements the rotor-position sensing required for FOC; it does not replace motor commutation feedback or eliminate mechanical compliance.

4.6.2 Sensor Selection and Mechanical Integration

Tunnelling magnetoresistance (TMR) is a candidate technology, with miniature Hall-based devices retained as alternatives. The TLE5501 is an example of a TMR angle sensor, while the Hall-based TLI493D-W2BW illustrates a smaller package option with typical dimensions of $1.13 \times 0.93 \times 0.59\,\text{mm}$ [24, 25]. These are evaluation candidates rather than selected components; chip dimensions exclude the magnet, PCB, connections, and required clearance. Selection will follow the installed angular-error budget, repeatability, measurement range, latency, temperature behavior, and total integration volume. Digital resolution alone does not establish angular accuracy.

Sensor and magnet placement must preserve the central tendon channels, joint bearings, and proposed reverse-bending range. Internal wiring requires strain relief and protection through the full motion envelope. Alignment, air-gap variation, nearby steel, and fields from neighboring magnets and motors must be evaluated in the assembled finger, including simultaneous motion of both MCP axes.

4.6.3 Software Calibration and Feedback

Calibration will associate measured joint angles with motor/spool position and tendon payout over the motion range, in both directions and under representative loads and pretensions. This mapping can supply feedforward motion commands, while joint-angle error drives an outer feedback loop around the motor's inner current loop. Feedback gains and bandwidth will be limited by tendon compliance, sensing delay, and the intended impedance so that position correction does not undermine compliant contact behavior. A persistent mismatch can flag transmission drift or slack, but angle measurements alone cannot uniquely determine tendon tension. Validation against an independent angle reference, as described in Section 6.4, will establish installed accuracy and propagation of joint-angle error into fingertip-position error. No sensor accuracy or closed-loop performance has yet been demonstrated for this assembly.

5 Tendon Materials and Transmission Qualification

5.1 Candidate Materials and Selection Rationale

Sufix 832 is the initial finger-tendon candidate based on favorable preliminary handling tests. Its stated construction combines seven HMPE fibres and one GORE performance fibre, with 32 weaves per inch [14]. This identifies the product construction; it does not establish its terminated strength, creep, or fatigue performance in the proposed mechanism. The wrist requires a separate line or belt selection against the larger loads calculated in Section 3.5.

Selection will balance loaded stiffness, sustained extension, recovery, bending fatigue, sliding wear, termination efficiency, diameter, and replaceability. Published comparisons include HMPE, aramid, liquid-crystal polymer, polyester, and polyamide, but differences in grade, braid, conditioning, and load prevent a universal material ranking. Appendix C retains the source-specific comparisons and screening protocol.

5.2 Braid Geometry and Construction

Interlacement, braid angle, pick count, strand count, and any core–cover structure affect how extension is divided between fibre strain and geometric rearrangement. Common interlacements are summarized in Table 11 [12].

A larger braid angle generally permits more axial extension through yarn reorientation before fibre extension dominates; increasing pick count changes compactness and internal contact. Strand count alone is not a stiffness or creep rating. A core–cover line can separate load-carrying and protective functions, while relative movement between layers and termination load transfer introduce additional variables [13]. Comparisons must therefore identify the actual construction rather than attributing all behavior to the polymer or nominal diameter.

Table 11: Common braid interlacement patterns.

Pattern	Yarn path
Diamond (1/1)	Alternates over one opposing yarn and under the next.
Regular (2/2)	Passes over two opposing yarns, then under two.
Hercules (3/3)	Passes over three opposing yarns, then under three.

5.2.1 Rationale for Testing the Finished Tendon

The installed tendon includes its braid, coating, termination, routing curvature, and preconditioning. These factors can dominate early settling and measured drift. Material data will guide candidate selection, while acceptance will depend on the complete routed and terminated assembly.

5.3 Creep, Constructional Settling, and Recovery

A useful test distinguishes the extension produced immediately by loading from additional extension during the load hold. In a braided tendon, measured extension can include both deformation of the constituent fibres and changes in braid geometry. Initial seating of crossings and terminations must therefore be recorded separately from subsequent drift. Recovery after unloading is a further measurement; small residual extension does not necessarily mean that a tendon remains dimensionally stable while loaded.

Let L_0 be the gauge length under a defined small reference tension before the load step, and let t_0 be the recorded time at which the target load is reached. Define

$$\varepsilon_{\mathrm{tot}}(t) = \frac{L(t) - L_0}{L_0}, \qquad \Delta\varepsilon_{\mathrm{hold}}(t) = \frac{L(t) - L(t_0)}{L_0}. \tag{11}$$

Report both quantities and the loading-ramp duration: the second excludes extension already accumulated by t_0, but does not by itself isolate molecular creep from continuing structural settling. After a specified recovery time t_r, measure residual strain at the original reference tension:

$$\varepsilon_{\mathrm{res}}(t_r) = \frac{L_{\mathrm{recovered}}(t_r) - L_0}{L_0}. \tag{12}$$

Finite-time residual strain should not automatically be called permanently unrecoverable strain. A complementary stress-relaxation test holds tendon length fixed and records the decrease in tension; this is relevant when the motor and joint remain stationary while pretension changes.

5.4 Guide Friction and Wear

The prototype contact is braided line against stainless-steel dowels. The capstan coefficient used in Section 3.3 is a literature-based sensitivity assumption, not a verified coefficient for Sufix 832. Measure branch tensions at a known wrap angle to obtain

$$\mu_{\mathrm{eff}} = \frac{\ln(T_{\mathrm{high}}/T_{\mathrm{low}})}{\beta}. \tag{13}$$

Characterize breakaway and steady sliding separately in both directions, recording dowel diameter, finish, load, speed, temperature, and contamination. Repeat after representative wear. Bearing-

supported guides will be evaluated through measured routing efficiency, bearing drag, minimum bend radius, and retained tendon strength rather than assigning them a sliding coefficient.

5.5 Qualification Strategy

The screening program compares as-received and preconditioned specimens under equal application loads and, separately, matched fractions of measured breaking force. Record immediate extension, hold strain, recovery, fixed-length tension decay, grip slip, and retained strength. Straight-line creep tests precede routed tests so bending and sliding effects can be identified. The detailed protocol in Appendix C includes 24-hour screening, seven-day follow-up holds, replication, and environmental records. Final service intervals will follow joint drift and transmission condition under the actual duty cycle.

6 Prototype Development and Verification

6.1 Staged Prototype Development

The first stage uses PLA structures, stainless-steel dowel guides, and forearm-mounted servos to establish joint geometry, tendon travel, pretension adjustment, and the detachable interface. The second stage substitutes the custom brushless actuator modules and bearing-supported routing while retaining the same joint and interface definitions. CNC-aluminum finger components follow dimensional and load validation. Each stage is compared using the same independent measurements; prototype feasibility does not establish the final actuator's thermal or durability rating.

6.2 Standards and Benchmarking Basis

ISO 9283 provides performance criteria and test methods for industrial manipulators, including accuracy and repeatability [3]. Its measurement principles will inform joint and fingertip testing. Adapted finger tests will be identified as project-specific procedures; adaptation alone does not establish conformity with the standard.

NIST end-effector benchmarking protocols provide methods for grasp strength, grasp cycle time, finger strength, and finger repeatability [4]. NIST assembly task boards provide complementary task-level benchmarks involving components such as screws, gears, connectors, wires, and belts [5]. These references provide a basis for reproducible evaluation, while additional tests address the particular behavior of the proposed tendon-driven hand.

6.3 Performance Test Matrix

Fixtures, trial counts, loads, speeds, and acceptance thresholds will be fixed before qualification. The matrix defines project-specific tests; the cited standards and protocols provide their measurement basis.

Table 12: Verification scope for the hand, wrist, and proximal rotation assembly.

Test	Required measurements
Motion and independence	Range, coupled motion, tracking error, settling time, and loaded speed for every axis. Include reverse finger bending, clearances, tendon engagement, both wrist axes, and proximal rotation.
Position and calibration	Independently measured accuracy and repeatability, directional hysteresis, warm-up drift, and changes after loading, retensioning, or hand replacement.
Force and torque	Calibrated fingertip/grasp force and wrist torque in all four directions; compare commanded values and motor-current estimates across postures and loads.
Backdrivability	Breakaway and running torque versus posture, speed, and pretension, with controller mode and powered state specified. Separate passive resistance from commanded compliance.
Thermal and endurance	Winding, electronics, and bearing temperatures; transmission losses, wear, retained tendon strength, maintenance frequency, and calibration drift over documented hours and cycles.
Interface and manipulation	Detach–reattach time and alignment repeatability; grasp and assembly success, completion time, slips, and dropped objects under fixed starting conditions.

6.4 Calibration and Independent Verification

Calibration establishes the joint references, motion limits, tendon pretension or belt installation tension, and actuator-to-joint mapping. Mechanical homing locates a repeatable datum; a stored offset relates that datum to the operating joint coordinate [26]. Motor electrical and rotor-sensor calibration remain separate from this mechanical procedure.

6.4.1 Homing References and Joint Coordinates

The proposed reference directions are listed in Table 13. Finger flexion uses straight as 0°, backward extension as negative, and forward flexion as positive. Thus, a mechanical stop approximately 45° beyond straight corresponds to about -45°, even if the motor's internal position counter is reset to zero there. The actual offset must be calibrated against the assembled geometry. Lateral axes may use their centered configuration as the operating zero, with the homing offset established independently.

Table 13: Proposed mechanical homing references. Final travel limits and offsets require verification on the assembled mechanism.

Controlled motion	**Proposed reference**
Finger flexion–extension	Maximum backward extension, initially targeted at approximately 45° beyond straight.
Finger MCP abduction–adduction	Maximum travel toward the designated left-hand side in a fixed hand reference frame.
Wrist flexion–extension	Maximum backward extension.
Wrist radial–ulnar deviation	Maximum travel toward the designated lateral side.
Thumb flexion and lateral axes	Corresponding extension or lateral reference for each axis, following the final thumb allocation.
Additional thumb rotation	Maximum clockwise rotation, with the viewing direction specified along the rotation axis.

Left/right and clockwise/counterclockwise must be defined in the assembly coordinate system, including the convention for mirrored hands. Home the two wrist axes separately, holding the other axis in a specified clearance-compatible pose, so a combined corner contact does not obscure which limit has been reached. Joint order and neighboring-joint poses must similarly avoid finger and thumb collisions.

6.4.2 Proposed Homing and Mapping Sequence

1. **Pretension the complete transmission.** Set and record tendon pretension throughout the hand using the ratchets before beginning finger homing. Set the wrist tendon pretension or belt installation tension as applicable. Support the hand and clear the motion envelope.

2. **Home one finger at a time.** Select one non-thumb finger and bring its DIP, PIP, and MCP flexion joints to their backward-extension references from Table 13. Approach each joint reference individually in a defined order, keeping the other joints in clearance-compatible poses. Use low speed and reduced torque or force where supported, with bounded search travel and a timeout.

3. **Measure and store each actuator's starting reference.** Gently seat the joint at its specified mechanical end stop. During operator-supervised setup, confirm that the joint is physically seated, then record the servo output-shaft angle or motor encoder position under a repeatable low seating load. The mechanical stop defines the joint datum, and the recorded actuator position becomes its stored starting reference; no separate limit switch is required. Use the actuator's available position feedback for the measurement, identifying the measured shaft and applicable reduction. Joint-sensor readings may also be logged when available. Reduce drive effort after recording to avoid sustained loading against the stop.

4. **Complete and verify the selected finger.** Back away and repeat each approach from the same direction to check reference repeatability. Home the MCP abduction–adduction axis separately at its designated lateral reference and record its servo angle in the same way. Each non-thumb finger therefore has four stored actuator references: three for flexion–extension and one for MCP lateral motion. Apply the calibrated offsets between these starting references and the operating joint zeros, then move the finger away from its limits.

5. **Repeat across the hand.** Complete the same procedure for each remaining non-thumb finger before homing the thumb axes and the two wrist axes at their respective references. Home the wrist axes separately. Save the per-axis reference angles, offsets, pretension settings, and applicable mechanical and controller configuration.

6. **Verify the motion calibration.** The stored starting angles establish the homing references; calibration of the motion between those references still requires measurements at several intermediate positions in both directions under defined pretension and representative loads. Fit the motor-to-joint mapping, quantify hysteresis, and verify coordinated motion and software limits. Recheck references and mapping after retensioning or hand replacement.

Fit parameters with a defined set of poses and loads, then validate against independent poses and loads using calibrated angle or optical measurements and load cells. Motor encoders, proposed joint sensors, and current estimates cannot serve as their own reference measurements. Report instrument uncertainty and distinguish positioning bias from trial-to-trial spread. Record mechanical revision, winding, reduction, spool geometry, firmware, and tension settings. Repeat verification after warm-up, sustained loading, and cycling; recalibration intervals follow measured drift.

6.5 Durability and Maintenance Qualification

A provisional 40,000 operating-hour planning horizon replaces the original ten-calendar-year objective. It is informed by model-specific industrial-robot service guidance [2], not a universal industrial-arm standard or a demonstrated service life for this hand. Qualification requires an explicit assembly mission profile specifying loads, motion ranges, speed, acceleration, hold time, cycle frequency, and temperature. Record operating hours and completed cycles separately; calendar duration alone does not define mechanical exposure.

Tendons, guides, bearings, and other wear items may require scheduled replacement before that horizon. Endurance tests will track heat, wear, transmission losses, tensioning frequency, and recalibration needs. Access and replacement time form part of the packaging evaluation. The long-term objective permits maintenance and does not require every original component to remain in service throughout the planning period.

6.6 Task-Level Reporting

Use defined grasp objects and assembly tasks with controlled geometry, friction, placement, and starting pose. Report trial count, success criteria, completion time, performance distribution, failures, and measurement uncertainty together with configuration and environmental conditions. Human-reference loads in Section 3 are sizing inputs; task-level human comparability requires its own matched test protocol. No experimental qualification results are claimed in this design report.

References

[1] ODrive Robotics, *Control*. ODrive control documentation.

[2] ABB Robotics, *Product manual—IRB 6620*, document 3HAC027151-001, revision AC, Section 3.2.1, p. 118. Maintenance intervals and overhaul benchmark.

[3] International Organization for Standardization, *ISO 9283:1998—Manipulating industrial robots: Performance criteria and related test methods*. Standard information.

[4] J. Falco et al., *Benchmarking Protocols for Evaluating Grasp Strength, Grasp Cycle Time, Finger Strength, and Finger Repeatability of Robot End-effectors*, IEEE Robotics and Automation Letters, vol. 5, no. 2, 2020. doi:10.1109/LRA.2020.2964164.

[5] K. Kimble et al., *Performance Measures to Benchmark the Grasping, Manipulation and Assembly of Deformable Objects Typical to Manufacturing Applications*, Frontiers in Robotics and AI, 2022. doi:10.3389/frobt.2022.999348.

[6] M. Shinohara, M. L. Latash, and V. M. Zatsiorsky, *Age effects on force produced by intrinsic and extrinsic hand muscles and finger interaction during MVC tasks*, Journal of Applied Physiology, vol. 95, no. 4, 2003. doi:10.1152/japplphysiol.00070.2003.

[7] M. Gautam, *Hybrid Composite Wires for Tensile Armour in Flexible Risers*, PhD thesis, University of Manchester, 2016, pp. 82–83. Dyneema fibre–stainless-steel friction measurement.

[8] S. K. Pal, V. B. Thakare, and G. Singh, *Creep behaviour of braided cordages made of high performance fibres for aerospace applications*, Indian Journal of Fibre & Textile Research, vol. 32, pp. 13–20, 2007. Publisher repository.

[9] P. Davies, Y. Reaud, L. Dussud, and P. Woerther, *Mechanical behaviour of HMPE and aramid fibre ropes for deep sea handling operations*, Ocean Engineering, vol. 38, pp. 2208–2214, 2011. doi:10.1016/j.oceaneng.2011.10.010.

[10] J. Zeng et al., *Mechanical behavior of synthetic fiber ropes for mooring floating offshore wind turbines*, PLOS ONE, vol. 20, e0318190, 2025. doi:10.1371/journal.pone.0318190.

[11] L. Civier et al., *Short and long term creep behaviour of polyamide ropes for mooring applications*, Ocean Engineering, vol. 259, 111800, 2022. doi:10.1016/j.oceaneng.2022.111800.

[12] T. Hamouda, N. M. Aly, and M. H. Elshakankery, *An experimental study on the interaction between braiding structural parameters and their effects on ropes mechanical properties*, Journal of Industrial Textiles, 2022 (first published online 2020). doi:10.1177/1528083720960732.

[13] Marlow Ropes, *Rope Construction*. Manufacturer construction guide.

[14] Rapala / Sufix, *832 Advanced Superline*. Manufacturer construction specifications.

[15] International Organization for Standardization, *ISO 2307:2019—Fibre ropes: Determination of certain physical and mechanical properties*. Standard information.

[16] ALVA Industries, *What Are Motor Winding Configurations?*, 2026. Winding and drive-selection tradeoffs.

[17] Allient, *A Guide to Custom Motors*. Custom winding and motor-constant considerations.

[18] maxon, *Strength of BLDC (EC) Motor with Sinusoidal Commutation*. Torque and current conventions.

[19] maxon, *Formulae Handbook*, Section 9.1, Thermal Behavior. Winding loss and temperature relations.

[20] R. Bhat, *Analyzing Electric Motor and Generator Designs with COMSOL*, COMSOL, 2021. Magnetic flux, yoke thickness, and torque analysis.

[21] S. L. Delp, A. E. Grierson, and T. S. Buchanan, *Maximum isometric moments generated by the wrist muscles in flexion-extension and radial-ulnar deviation*, Journal of Biomechanics, vol. 29, no. 10, pp. 1371–1375, 1996. doi:10.1016/0021-9290(96)00029-2; Author-hosted paper.

[22] Gates, *Light Power and Precision Drive Design Manual*. Synchronous-belt sizing and installation guidance.

[23] Gates, *PowerGrip GT3 Drive Design Manual*. Belt-drive design and positioning considerations.

[24] Infineon Technologies, *TLE5501 E0001: TMR-based angle sensor*. Manufacturer product information.

[25] Infineon Technologies, *TLI493D-W2BW: 3D magnetic sensor*. Manufacturer documentation and package dimensions.

[26] ODrive Robotics, *Endstops/Homing*. Reference detection, homing offsets, and operating zero.

A Extended Calculations and Sensitivity

A.1 Guide-Loss Sensitivity

For the 30 N MCP reference case in Section 3.4, exploratory static coefficients 0.05, 0.10, and 0.15 produce required motor torques of approximately 0.625, 0.736, and 0.865 N m, respectively. These are sensitivity inputs, not measured Sufix 832 values or a validated uncertainty interval. Increasing wrap angle also raises the predicted loss exponentially.

Removing guide losses entirely gives an ideal lower bound of 0.529 N m for the MCP reference motor torque, with the same gearbox efficiency and safety factor. This is not a predicted ball-bearing result. Measured bearing, seal, and tendon bending losses must be added to assess how closely the proposed rolling guides approach that limit.

For comparison, applying the explicit two-branch dowel model to the wrist with $\mu = 0.071$, $\beta = \pi$, $T_p = 25$ N, $r_w = 30$ mm, $r_s = 10$ mm, $G = 6$, $\eta_g = 0.85$, and $SF = 1.5$ gives approximately 1.528 N m at the reference flexion load and 3.023 N m at twice that load. These are alternative prototype routing cases; they do not include the separate $\eta_t = 0.90$ allowance used for the rolling-route baseline.

A.2 Ideal Rewinding and Nonideal Copper Loss

For an ideal rewind of the same magnetic geometry at constant copper fill and temperature, increasing turns by a factor a gives approximately $K_t \propto a$, $K_V \propto 1/a$, and $R_\phi \propto a^2$. Current at equal torque falls as $1/a$, so copper loss is unchanged. This scaling assumes comparable end turns and negligible changes in other loss mechanisms.

A.2.1 Worked Comparison at the Human-Reference Torque

Use the rounded required motor torque $\tau_m = 0.670$ N m from the 30 N MCP example in Section 3.4; its reduction, transmission assumptions, and safety factor are already included. Compare ideal 100, 200, and 400 K_V rewinds. Assume a star-connected motor with $R_\phi = 0.050\,\Omega$ for the 200 K_V case, scaled as above at the same reference temperature. For balanced sinusoidal currents,

$$P_{\mathrm{Cu}} = 3R_\phi I_{\phi,\mathrm{rms}}^2 = \frac{3}{2} R_\phi I_q^2, \qquad I_{\phi,\mathrm{rms}} = \frac{I_q}{\sqrt{2}}. \tag{14}$$

This follows by summing the three phase copper losses. A star winding's measured line-to-line resistance is $2R_\phi$; it must not be substituted as the phase resistance. Copper-loss estimation also requires resistance at operating temperature [19].

Table 14: Illustrative rewinds delivering the same motor torque.

Quantity	**100** K_V	**200** K_V	**400** K_V
Torque constant K_t (N m/A)	0.08270	0.04135	0.02068
Current I_q for 0.670 N m (A)	8.10	16.20	32.41
Assumed phase resistance (Ω)	0.2000	0.0500	0.0125
Total copper loss (W)	19.69	19.69	19.69
Torque at an illustrative 10 A I_q limit (N m)	0.827	0.414	0.207

For the 100 K_V case, $I_q = 0.670/0.08270 = 8.10\,\text{A}$ and $P_{\text{Cu}} = 1.5(0.200)(8.10)^2 \approx 19.69\,\text{W}$. The higher-$K_V$ cases need more current but have proportionally lower resistance. At a hypothetical 10 A peak-current limit, only the 100 K_V case reaches the target torque. This is a drive-current comparison, not proof that its winding can sustain that torque thermally or reach the required speed.

A.2.2 When a Lower-K_V Winding Can Lose Efficiency

A lower-K_V rewind can be less efficient if its actual resistance rises more than the ideal scaling predicts, for example because the usable copper fill decreases or end turns become longer. Suppose the 100 K_V winding instead measures $0.260\,\Omega$ per phase while retaining the assumed K_t. At the same torque, current remains 8.10 A, but copper loss becomes approximately 25.60 W, a 30% increase. The penalty comes from the poorer resistance-to-torque relationship, rather than from lower K_V alone.

As a separate illustrative operating point, combine 0.670 N m with 240 RPM:

$$P_{\text{mech}} = \tau_m \frac{2\pi n_m}{60} \approx 16.84\,\text{W}, \qquad \eta_{\text{Cu-only}} = \frac{P_{\text{mech}}}{P_{\text{mech}} + P_{\text{Cu}}}. \tag{15}$$

The ideal rewinds all give about 46.1% on this copper-loss-only basis; the higher-resistance example gives about 39.7%. These are calculated upper bounds within the assumed loss model, excluding iron, mechanical, drive, cable, and downstream transmission losses. They do not establish simultaneous torque–speed capability. At a stationary grasp, mechanical output power is zero even though current continues to heat the windings, so allowable holding torque must be determined thermally.

A.3 Stator Geometry Sweep

Using Equation (10), approximate the air-gap diameter by the stator outer diameter D_s for an initial screen. Detailed design must replace this approximation with the actual air gap. Relative $D_s^2 L_s$ in Table 15 is normalized to a 50 mm diameter and 15 mm stack. Required shear stress is a design demand, not a demonstrated motor capability.

Table 15: Proposed stator geometry sweep for a 0.670 N m motor target.

D_s (mm)	L_s (mm)	Relative $D_s^2 L_s$	Required stress (kPa)
40	10	0.427	26.66
50	10	0.667	17.06
50	15	1.000	11.37
60	10	0.960	11.85
60	15	1.440	7.90

A.4 Winding and Resistance Sweep

Tables 17 and 18 use the peak-current convention defined in Section 3.7. Resistance limits apply at operating temperature under the stated copper-loss budgets. They exclude iron, bearing, controller, and cable losses. The wrist upper target doubles torque; at unchanged resistance it produces four times the reference copper loss.

Table 16: Candidate active stator geometries for the governing wrist flexion load. Stress is required loading, not demonstrated capability.

Diameter (mm)	**Stack (mm)**	**Stress at 1.329 N m (kPa)**	**Stress at 2.658 N m (kPa)**
70	20	8.63	17.27
80	15	8.81	17.63
80	20	6.61	13.22
90	20	5.22	10.45

Table 17: Winding candidates at equal target torque and an assumed 15 W copper-loss limit.

K_V **(RPM/V)**	K_t **(N m/A)**	I_q **(A)**	**Maximum hot phase resistance** (Ω)
60	0.1378	4.86	0.423
80	0.1034	6.48	0.238
100	0.0827	8.10	0.152

Table 18: Wrist winding comparison using an assumed 25 W motor copper-loss budget at the reference load.

K_V	K_t **(N m/A)**	I_q**, ref. (A)**	I_q**, above (A)**	**Max. hot phase** R (Ω)
40	0.2068	6.43	12.86	0.403
60	0.1378	9.64	19.28	0.179
80	0.1034	12.86	25.71	0.101

B Calculated Sensitivity Plots

The following plots isolate the effects of spool radius, fingertip force, and tendon moment arm under the finger assumptions in Table 2: $\mu = 0.071$, total wrap $\beta = \pi$, return-branch joint tension $T_p = 10$ N, gearbox ratio $G = 5$, efficiency $\eta_g = 0.85$, and safety factor $SF = 1.5$. All plotted torques are at the motor shaft before reduction. They are calculations, not measured actuator performance.

The branch-friction model retains a nonzero tension-loss allowance at zero fingertip load; that intercept is not a measured no-load motor torque. The MCP flexion and lateral curves coincide only because the assumed external moment arms are equal.

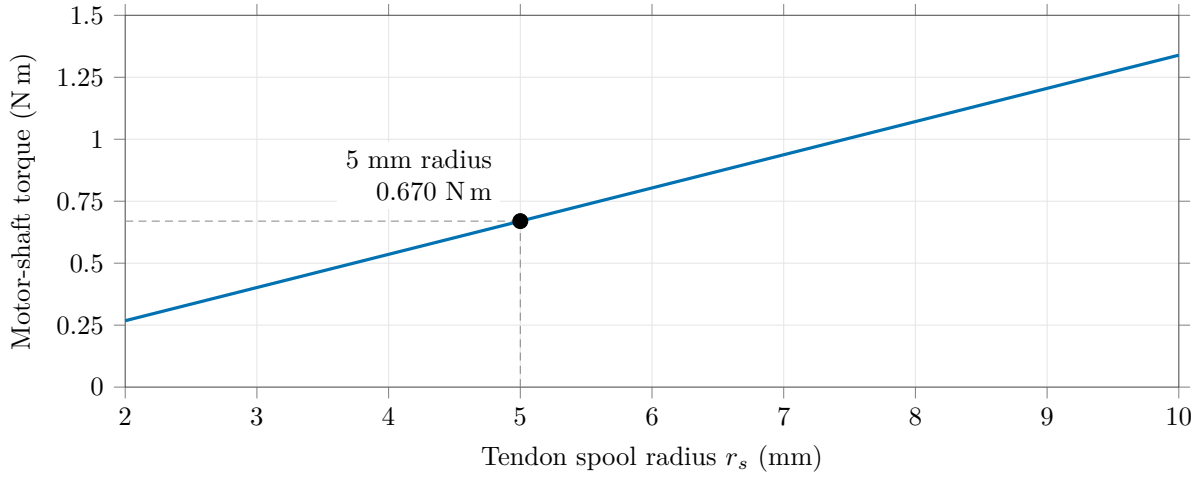


Figure 1: Calculated motor torque versus spool radius for the 30 N MCP example, with an 80 mm external moment arm and 8 mm tendon moment arm. The marked 5 mm radius corresponds to a 10 mm tendon winding diameter. All points include the shared friction, gearing, and safety-factor assumptions stated in this appendix.

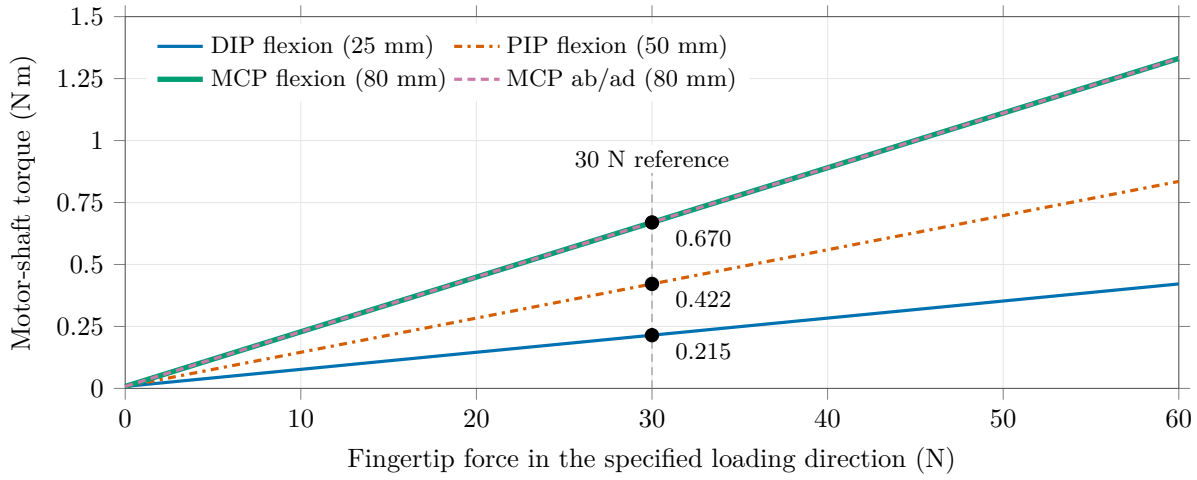


Figure 2: Calculated motor torque versus fingertip force; legend distances are assumed external moment arms. Markers identify the 30 N cases. The two MCP curves coincide because their assumed leverage and transmission are identical. Sideways loading is a separate design case; its 30 N value is not a human-strength benchmark.

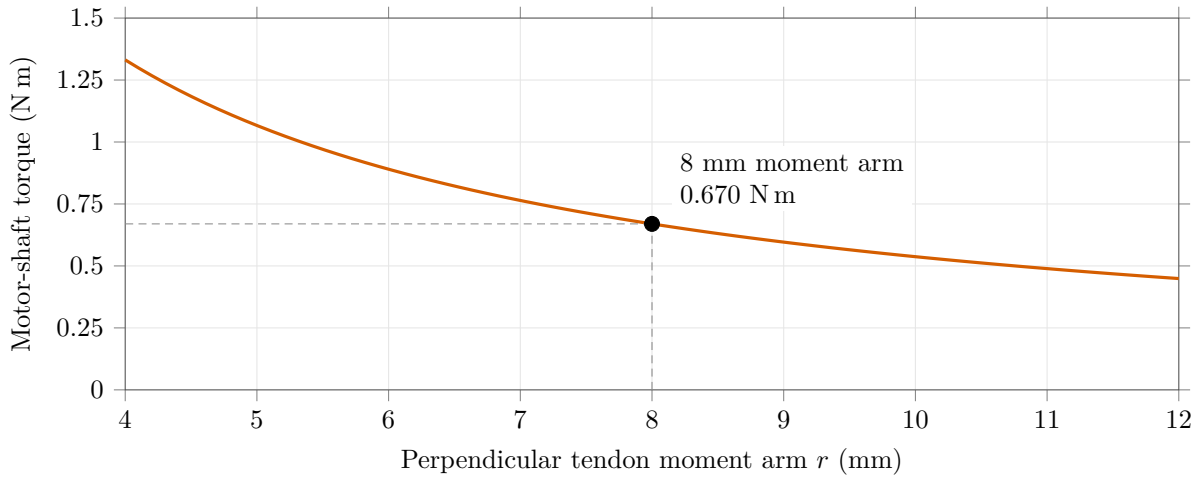


Figure 3: Calculated motor torque versus perpendicular tendon moment arm for the 30 N MCP example. External moment arm is fixed at 80 mm and spool radius at 5 mm. The marked 8 mm reference gives 0.670 N m before reduction; other friction and transmission assumptions remain fixed.

C Supporting Tendon Evidence and Test Protocol

C.1 Published Studies Across Tendon Materials

No single result establishes a universal ranking for all strings. The following studies collectively cover UHMWPE/HMPE, liquid-crystal polymer, polyamide, polyester, and aramid. Their specimen sizes, loads, temperatures, and conditioning differ, so their numerical results should not be combined into a common ranking without matched tests.

Table 19: Selected experimental literature relevant to tendon creep.

Study	Materials and conditions	Finding and relevance
Pal et al. (2007) [8]	Braided Dyneema SK75, Spectra 1000, Vectran, and untreated/heat-set nylon 66; sustained loads and recovery over days.	Direct cordage comparison. Vectran and nylon recovered more favorably than the tested polyethylene cords; heat setting improved the nylon response. Loading and recovery durations differed between material groups.
Davies et al. (2011) [9]	HMPE and aramid; single-fibre and large braided-rope measurements, including six-hour creep holds at 20 °C.	Aramid crept less in those tests. HMPE stiffness increased substantially after bedding-in. Results identify mechanisms but do not directly predict small fishing-line behavior.
Zeng et al. (2025) [10]	Polyester and nylon marine ropes; conditioning and stepped holds at 30, 45, and 60% of minimum breaking strength.	Nylon showed greater strain and creep rate than polyester in the reported tests. Load history and conditioning affected stiffness and recovery; these were relatively short holds.
Civier et al. (2022) [11]	Polyamide 6 sub-ropes in water; long-term creep tests lasting two years.	Demonstrates the scale of sustained testing available in marine-rope research. The wet sub-rope results are not a lifetime rating for a dry robotic tendon.

C.1.1 A Quantitative Cordage Comparison

Pal et al. tested Spectra 1000 and Vectran at 32% of specified breaking strength for approximately 22 days, followed by 25 days of recovery, over a reported temperature range of 22–40 °C. Total loaded elongations were about 9.7% and 3.06%, respectively; these include the initial extension. Residual extensions were about 8.25% and 0.93%. These are specimen-specific results, not expected values for Sufix 832. Equal fractions of breaking strength also do not imply equal material stress [8].

For selection, compare operating-load stiffness, additional hold strain, recovery, and retained strength independently. A material with good recovery can still cause unacceptable joint deflection while loaded. Conversely, high initial stiffness does not establish low long-term creep. Modern fibre grades,

coatings, braid construction, and processing must be identified rather than transferring a result to every product in the same polymer family.

C.2 Proposed Comparative Test Program

The comparative program will test Sufix 832, an identified alternative HMPE grade, a Vectran line, an aramid line, polyester, and nylon. Availability at the required diameter and reliable terminations will determine the final specimens. The following values are proposed screening conditions, not a published qualification standard:

1. **Document and condition specimens.** Record manufacturer, fibre grade, diameter, construction, finish, gauge length, and termination. Use at least three specimens per screening condition, increasing replication when variability warrants it. Record temperature and humidity continuously; compare an as-received set with a separately preconditioned set to quantify initial settling.

2. **Use two load comparisons.** Test at the same intended operating tension to compare candidate tendons for the hand, and separately at matched fractions of measured breaking force to compare relative material utilization. An initial fractional-load screen may use 10, 20, and 30%, subject to specimen and fixture capacity. Include the actual continuous pretension and sustained grasp loads; a fishing-line label alone is not a measured strength for the terminated assembly.

3. **Measure sustained extension.** Begin with a 24-hour screen and extend promising candidates to seven-day holds and longer service-representative tests. Use a controlled tensile load with direct gauge-length measurement, rather than relying only on machine or motor displacement. Log densely during loading, then at increasing time intervals. Track grip slip separately.

4. **Measure recovery and pretension loss.** After each hold, return to the reference tension and record recovery for at least 24 hours, extending observation if it continues. Run a separate fixed-length relaxation test. Compare residual breaking force on tested specimens with unexposed controls.

5. **Evaluate the routed assembly.** After straight-line characterization, repeat representative conditions with stainless-steel dowels and bearing-supported pulleys. Measure both tendon branches, joint drift, and loss of pretension. Keep bending fatigue and sliding wear tests distinct from constant-load creep, then combine them in the service-duty test.

ISO 2307:2019 provides methods for properties including diameter, braid pitch, elongation, and breaking force [15]. It is a useful basis for specimen characterization; citing it does not make the proposed sustained-load program a standardized creep qualification. Any departures needed for very small tendons will be documented.

C.3 Implications for Calibration and Tensioning

Report extension in both millimetres and strain, together with load, temperature, elapsed time, and recovery time. As a geometric illustration, 0.1% extension over a 500 mm tendon path is 0.5 mm. If uncompensated length change were taken up solely by rotation about a constant 8 mm moment arm, its equivalent angle would be $0.5/8 = 0.0625$ radians, or about 3.6°. This is a sensitivity example,

not a prediction of the antagonistic assembly: matched extension in both branches may chiefly reduce pretension, whereas unequal extension may also shift joint position.

Acceptance limits will be derived from allowable joint error, pretension loss, tensioner travel, and recalibration interval. Ratcheting can remove accumulated slack, but it does not remove load-dependent compliance, continuing creep, or loss of material strength. The final tendon choice will balance measured dimensional stability with friction, bending life, mass, and termination reliability.

D ActuationLab Calculator Reference

ActuationLab implements the force-analysis and preliminary outrunner-sizing methods developed in this paper. The force workspace maps a specified load to joint torque, tendon tension, and actuator demand, or reverses the calculation to estimate load capacity. The motor workspace examines the current, copper heating, geometry, winding, and reduction associated with a selected shaft-torque requirement. All inputs remain editable assumptions; example presets are not validated hardware ratings. The website and paper are maintained separately.

D.1 Force Workspace: Inputs and Workflow

Select the assembly and load, enter posture and transmission geometry, then inspect each axis. Carry the selected axis's *required shaft torque*, which already includes the design factor, into the motor workspace. Motor speed is gear reduction multiplied by spool speed. Optional material checks require measured properties rather than a material name alone.

Control or input	**Definition and units**
Assembly; solve mode	Finger: MCP, PIP, and DIP flexion plus MCP lateral motion. Wrist: one selected wrist motion. Solve from an applied load, or reverse the calculation using available shaft torque.
Fingertip force; force angles	Force magnitude in N. In-plane angle: 0° along global $+x$, 90° along $+y$. Lateral angle: 90° along $+z$. Direction remains global as posture changes.
Wrist motion; applied torque	Select flexion, extension, radial deviation, or ulnar deviation and enter external joint torque in N m. Proximal forearm rotation is outside this calculation.
Segment lengths	Proximal, middle, and distal lengths in mm: MCP–PIP, PIP–DIP, and DIP–tip. They establish joint centers and external-force leverage.
Joint posture	MCP, PIP, and DIP relative flexion angles and MCP abduction in degrees. Zero flexion gives a straight finger; successive relative angles set segment orientation.
Guide-loss model	Choose capstan losses over sliding dowels or an aggregate rolling-guide/belt efficiency. These are alternative models, not compounded corrections.
Friction; guide wrap	Coefficient μ and total contact angle in degrees *per branch*; the same wrap is assumed for both branches. This is guide wrap, not attachment turns around the take-up horn.
Routing efficiency	η_t, a fraction between zero and one, replaces the capstan model. It sizes torque but does not resolve individual spool-side branch tensions.
Joint-side return tension	Maintained releasing-branch tension in N. Pulling tension adds the load-induced difference. This is not a simulation of fixed initial pretension redistributing through elastic tendons.
Reduction; efficiency	G = motor speed/spool speed; enter 5 for a 5:1 reduction. Gear efficiency η_g is a fraction, separate from routing losses.
Design factor	$SF \geq 1$ multiplies total spool-torque demand. Nominal joint torques and nominal branch tensions remain unscaled. The design-tension check instead scales the load-induced tension increment while retaining return tension.
Per-axis tendon arm; spool radius	r and r_s in mm. The tendon arm is the perpendicular distance to its line of action, not generally the dowel-center offset. The spool radius is its effective winding radius. Both are treated as constant.
Available shaft torque; joint travel	Per-axis torque in N m *before reduction* is used for inverse capacity. Travel in degrees is a move magnitude, distinct from the current joint posture. Move duration in s gives average speed.
Material; optional properties	Material selection labels the case. Optional diameter (mm), terminated breaking force (N), and finished-line axial rigidity EA (N) enable stress, strength-ratio, and elastic-extension checks.
Path length; hold strain	Loaded path length in mm; optional additional hold strain in percent (enter 1 for 1%). Strain must come from a stated load, duration, temperature, and conditioning history. Blank optional inputs mean unknown, not zero.
Inspect axis	Selects the calculation steps and material checks to display without altering the other axes or the load case.

D.2 Force Workspace: Results and Interpretation

The signed joint moments follow the chosen axes and load direction; transmission sizing uses their magnitudes. The schematic is a projection of the three-dimensional finger calculation, not a tendon-routing drawing.

Result	Interpretation
Governing shaft torque	Largest required actuator-shaft torque among the modeled axes, in N m, after losses and SF. It is a motor requirement before gearing, not joint torque.
Available force or wrist torque	Inverse capacity in N or N m under the same allowances. The most constrained axis is identified. Finger capacity applies only at the entered posture and force direction.
External arm; joint torque	External arm in mm is the magnitude of projected joint moment per unit force, distinct from the tendon arm. Signed joint torque and the largest joint-torque magnitude are nominal load moments in N m.
Tension difference; joint branches	$\Delta T = \lvert\tau\rvert / r$ in N. Joint pulling tension is return tension plus ΔT; the returning branch retains the entered tension.
Spool branch tensions	Capstan model only: pulling tension is multiplied by $k = \exp(\mu\theta)$ and returning tension divided by k, with θ in radians. Aggregate efficiency cannot determine these individual tensions.
Peak nominal tendon tension	Largest nominal spool-side pulling tension for dowels. For aggregate efficiency, it is only the largest joint-side pulling tension, not an established maximum along the entire route.
Required spool; shaft torque	Spool torque includes routing loss and SF. Dividing by $G\eta_g$ gives required shaft torque. Both are in N m. The CSV also reports nominal spool torque before SF.
Design pulling tension	Applies SF to the load-induced tension increment while retaining return tension. Reported at the spool for dowels and at the joint for aggregate efficiency.
Breaking-force ratio; stress	Terminated breaking force divided by design pulling tension is a comparison, not a qualified working-load rating. Envelope stress (MPa) uses nominal diameter as a solid circle and is not actual fibre stress.
Elastic; hold extension	Elastic extension (mm) is nominal pulling tension times path length divided by EA, assuming uniform tension and linear rigidity. Additional hold extension is path length times the entered strain fraction.
Equivalent angular drift	Hold extension divided by r, converted to degrees, assumes one uncompensated branch. Similar creep in both branches can reduce pretension instead of rotating the joint.
Travel; rotation; speed	Tendon travel (mm) is r times joint travel in radians. Spool rotation (degrees) is joint travel times r/r_s. Average spool rpm follows from move duration; motor rpm is G times larger. Peak speed and acceleration are not inferred.
Total ratio	Motor-to-joint motion ratio $N = Gr/r_s$, including both gearing and tendon leverage.
Plot; calculation steps	Sensitivity curves vary external load with posture and transmission assumptions fixed. The selected-axis steps show joint moment, tension difference, routing loss, spool demand, and shaft demand.

Inverse-result boundaries. "Insufficient" indicates that available shaft torque does not cover the capstan model's zero-load allowance. "Not bounded by joint-torque model" means the chosen force creates no moment about the modeled axes; it does not imply unlimited structural strength.

Presets and records. Finger presets supply lower, reference, upper, and lateral load cases; wrist presets provide the paper reference, scaled comparisons, and a timing-belt case. They are comparison assumptions rather than continuous human or hardware ratings. Selecting a preset or Reset restores its associated settings; editing produces a custom case. Results CSV exports numerical results with units, and Calculation record exports inputs and outputs as JSON. The selected-axis force case can be carried to motor sizing; neither workspace changes Overleaf automatically.

Scope. The force model assumes quasi-static loading, one fingertip point force or one wrist torque, independent antagonistic pairs, and constant effective radii. It excludes impacts, acceleration, gravity, multiple contacts, structural failure, cross-joint routing changes, and coupled compliance. Material names do not assign universal friction, strength, or creep properties.

D.3 Motor Workspace: Inputs and Conventions

The motor calculation uses balanced sinusoidal phases, zero direct-axis current, and *peak quadrature-axis current*. Its approximate torque-constant convention is $K_t = 8.27/K_V$. This current is neither phase RMS current nor DC supply current. Line-to-line resistance is converted to phase resistance only for a balanced star/wye winding.

Input	Definition and units
Target shaft torque; speed	Motor-shaft torque in N m before reduction, and mechanical rotor speed in rpm. A target transferred from force analysis already includes its SF; the motor workspace does not apply a second design factor.
Motor K_V	Speed constant in rpm/V for the proposed winding. Lower K_V raises torque per amp under the stated convention, but does not by itself establish greater continuous torque or efficiency.
Bus voltage; current limit	DC inverter-supply voltage in V and chosen peak q-axis current limit in A. The current limit must reflect the intended motor/controller combination; it is not a battery-current limit.
Resistance; measurement basis	Hot winding resistance in Ω, entered per phase or line-to-line. For a balanced star winding, phase resistance is half the line-to-line value. No temperature correction is performed; delta data require conversion outside this model.
Copper-loss budget	Assumed allowable winding heating in W. Requires justification by thermal analysis and testing; it is not output power, total loss, or a measured continuous rating.
Stator outside diameter	Diameter in mm of the active stator, not the complete housing. It approximates air-gap diameter when the latter is omitted.
Air-gap diameter	Optional diameter in mm of the cylindrical electromagnetic interaction surface, distinct from radial gap thickness. An explicit value replaces the stator-diameter approximation for the selected design.
Active stack length	Axial length in mm of the active laminated stator stack, excluding end turns, bearings, and casing.
Slots; magnet poles	Stator-slot count and even total rotor-pole count; poles are twice pole pairs. These describe candidate topology without proving winding feasibility, winding factor, or cogging performance.
Reduction; gear efficiency	Motor-to-spool ratio G and efficiency η_g. They relate the already entered shaft requirement to downstream torque and speed; editing them does not recompute external-load demand.
Joint arm; spool radius	Effective r and r_s in mm, with the same meanings as the force workspace. Together with G, they set the total ratio used for motion and inertia reflection.
Rotor inertia	Optional rotor moment of inertia in $\mathrm{kg\,m^2}$. Enter a measured or independently calculated value; the site does not infer it from motor diameter or mass.
Reference winding K_V; resistance	Baseline K_V in rpm/V and hot *phase* resistance in Ω for rewind comparisons. Reference resistance remains per-phase even when the main operating-point resistance is entered line-to-line.
Rewind resistance multiplier	Dimensionless correction multiplying ideal rewind resistance; 1 retains the fixed-fill reference scaling. It can explore departures caused by changed fill or end-turn geometry.
Reference turns; conductor diameter	Optional integer turns per coil and bare-wire diameter in mm. They enable comparative turns and diameter estimates for unchanged connection and strand count; insulation and practical packing are excluded.

Reading the comparisons. The main operating point uses the *entered* resistance. Rewind comparisons use the separate reference winding, so their predicted resistance and loss need not match the main result. The diameter plot holds target torque and stack length fixed; the current plot holds target torque fixed. Candidate-geometry rows approximate air-gap diameter by stator diameter except for an explicitly specified selected design.

Further design variables. The Proposed Actuator and Control Design section addresses the rationale for the outrunner architecture. Magnet properties, radial gap, back iron, teeth, laminations, winding layout, parallel strands, fill, insulation, cooling, bearings, retention, and control bandwidth require additional analysis. The calculator does not assign unsupported numerical torque gains to these choices.

D.4 Motor Workspace: Results and Limitations

Result	Interpretation
Torque constant; current	K_t in N m/A uses the peak q-axis convention. Required current is $I_q = \tau/K_t$; phase RMS current is $I_q/\sqrt{2}$ for the assumed sinusoidal phases. Neither is DC bus current.
Hot phase resistance	Normalized phase resistance in Ω, obtained directly or as half the line-to-line input for a balanced star winding. All main copper-loss calculations use this phase value.

Result	Interpretation
Copper loss; resistance ceiling	Winding heating is $1.5R_{\text{phase}}I_q^2$ in W. The maximum hot phase resistance allowed by the entered copper budget is $P_{\text{budget}}/(1.5I_q^2)$; the zero-torque case has no finite resistance ceiling from this check.
Motor constant; required minimum	$K_m = K_t/\sqrt{1.5R_{\text{phase}}}$ in $\text{N m}/\sqrt{\text{W}}$ expresses torque relative to copper heating. The budget-based minimum is $\tau/\sqrt{P_{\text{budget}}}$.
Current- and copper-limited torque	$K_t I_{\text{limit}}$ and $K_t\sqrt{P_{\text{budget}}/(1.5R_{\text{phase}})}$ in N m. These are screening ceilings, not verified peak or continuous ratings. Voltage, saturation, and thermal limits may impose tighter bounds.
Power; copper-only efficiency	Mechanical power is $\tau(2\pi n/60)$ in W. The copper-only fraction is output power divided by output power plus copper loss. It omits iron, drive, bearing, cable, and transmission losses and is not total system efficiency.
Speed proxy; electrical frequency	$K_V V$ in rpm is an approximate no-load proxy, not loaded-speed feasibility. Electrical frequency is mechanical rpm times total poles divided by 120, in Hz.
Required air-gap shear	Average tangential stress required for target torque, reported in kPa, using effective air-gap diameter and active stack length. It scales as $\tau/(D_g^2 L)$ and is a demand, not predicted magnetic capability.
Spool torque; speed; total ratio	Spool torque is $\tau G\eta_g$ in N m and spool rpm is shaft rpm divided by G. Total motor-to-joint motion ratio is $N = Gr/r_s$. The spool result does not include tendon-routing losses.
Reflected rotor inertia	$N^2 J_{\text{rotor}}$ in kg m^2 at the joint, when rotor inertia is supplied. Gear, spool, and structural inertia are not included. This quantity alone does not establish backdrivability.
Rewind factor; resistance	Turn multiplier $\alpha = K_{V,\text{ref}}/K_V$. Ideal phase resistance scales by α^2; the entered resistance multiplier then adjusts it. Comparison currents and copper losses use this hypothetical winding, not the main resistance input.
Turns; wire size	Estimated turns scale by α, conductor area by $1/\alpha$, and diameter by $1/\sqrt{\alpha}$ for fixed fill and unchanged strand count. Absolute turns and diameter require the optional reference inputs. Fractional results require a realizable winding redesign.
Comparison tables; checks	Speed-constant rows compare K_t, current, the resistance ceiling, and hypothetical rewind resistance and heating. Geometry rows compare required shear at the same torque. Checks flag exceeded assumptions; passing is not hardware qualification.

Efficiency and validation. At fixed geometry, copper fill, connection, mean turn length, and temperature, ideal rewinding reduces current while raising resistance; copper loss at equal torque is approximately unchanged. Lower K_V alone therefore establishes neither an efficiency penalty nor an efficiency advantage. The main calculation assumes linear torque per amp and omits saturation and ripple. It does not predict winding temperature, cooling capacity, loaded torque–speed performance, fatigue life, or impact survival. Verify these through magnetic/thermal analysis and prototype measurements.

Reproducibility. Motor presets are editable paper examples. Results CSV exports a numerical summary; Calculation record exports comprehensive inputs and calculated outputs as JSON. Retain current convention, resistance basis and temperature, source of the copper budget, and geometry assumptions with each comparison. The approximate torque-constant convention follows ODrive documentation [1]; it does not imply the proposed custom controller uses that hardware.